View metadata, citation and similar papers at core.ac.uk

brought to you by CORE

provided by Elsevier - Publisher Connector

Available online at www.sciencedirect.com

ScienceDirect

Physics Procedia 78 (2015) 210 – 221

Physics Procedia

15th Nordic Laser Materials Processing Conference, Nolamp 15, 25-27 August 2015, Lappeenranta, Finland

Mechanical properties of laser beam welded ultra-high strength chromium steel with martensitic microstructure

Martin Dahmen[a]*, Vitalij Janzen[b], Stefan Lindner[c], Rainer Wagener[d]

[a]*Fraunhofer Institute for Laser Technology, Germany*
[b]*Laboratory for Materials and Joining Technology, University of Paderborn,Germany*
[c]*Outokumpu Nirosta GmbH, Krefeld, Germany*
[d]*Fraunhofer Institute for Structural Durability and System Reliability LBF, Darmstadt, Germany*

Abstract

A new class of steels is going to be introduced into sheet manufacturing. Stainless ferritic and martensitic steels open up opportunities for sheet metal fabrication including hot stamping. A strength of up to 2 GPa at a fracture strain of 15% can be attained. Welding of these materials became apparently a challenge. Energy-reduced welding methods with in-situ heat treatment are required in order to ensure the delicate and complex heat control. Laser beam welding is the joining technique of choice to supply minimum heat input to the fusion process and to apply an efficient heat control. For two application cases, production of tailored blanks in as-rolled condition and welding in assembly in hot stamped conditions, welding processes have been developed. The welding suitability is shown in metallurgical investigations of the welds. Crash tests based on the KSII concept as well as fatigue tests prove the applicability of the joining method. For the case of assembly also joining with deep drawing and manganese boron steel was taken into consideration. The strength of the joint is determined by the weaker partner but can benefit from its ductility.

© 2015 The Authors. Published by Elsevier B.V. This is an open access article under the CC BY-NC-ND license (http://creativecommons.org/licenses/by-nc-nd/4.0/).

Peer-review under responsibility of the Lappeenranta University of Technology (LUT)

Keywords: Martensitic stainless steels; press hardening; welding; welding metallurgy; fatigue strength; structural strength

* Corresponding author. Tel.: +49 241 8906 607; fax: +49 241 8906 121.
E-mail address: martin.dahmen@ilt.fraunhofer.de

1875-3892 © 2015 The Authors. Published by Elsevier B.V. This is an open access article under the CC BY-NC-ND license (http://creativecommons.org/licenses/by-nc-nd/4.0/).
Peer-review under responsibility of the Lappeenranta University of Technology (LUT)
doi:10.1016/j.phpro.2015.11.031

1. Introduction

The requirement on materials and resource efficiency of vehicles, chemical equipment, and machines are obtained by improved product design, increased strength of the materials applied, and by application of novel manufacturing technologies. Martensitic stainless steels offer great opportunities for lightweight construction. They show interesting properties especially at highest strengths. In hardened state an ultimate tensile strength between 1000 and 2000 MPa can be attained.

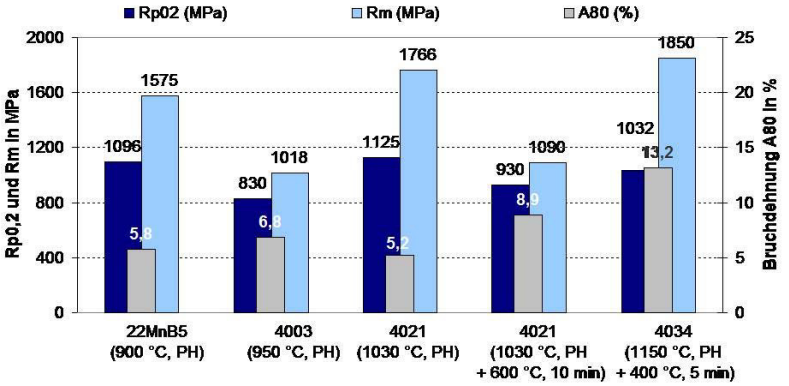

Fig. 1. Mechanical properties of different press hardenable steels

The weldability of ferritic-martensitic and martensitic steels is rated as limited. Especially for the press hardened materials, there are no process settings available. Laser beam welding, characterized by low heat input, in combination with in situ heat treatment offers great potential for joining these steel grades with high joint quality and sufficient joint performance (Costa et al. 2003). In previous research work the welding suitability could be demonstrated (Dahmen et al. 2014, 2012).

Nomenclature

AR	as rolled
HAZ	heat-affected zone
PH	press hardened
QS	quasi-static load application
SA	crash load application

Because of some of the investigated materials are considered to be non weldable, especially in hot formed state, welding suitability was tested and assessed. Starting with an overview of the investigated steels with about 13 wt.% chromium and carbon contents varying between 0.08 and 0.46 wt.%, the results for welding parameterization (e.g., annealing) and its influence on metallurgy of welds in as rolled (AR) and press hardened (PH) state as well as of welds after hot stamping are appraised. Furthermore, a first assessment of the strength and the effect of processing parameters is done by hardness surveys. The result of the basic investigation fit well with the properties represented in figure 1. The low-carbon ferrite delivers low strength, and the ferritic-martensitic 1.4021 shows a high fluctuation in the results which require special attention and further research. The most promising candidate, with view to the maximum strength achievable, is the high carbon containing 1.4034 (X46Cr13). The current contribution will focus on this material.

For the evaluation of the joint strength of square butt joints fatigue test were undertaken. Many welded structures are loaded cyclically in service. The different process sequences and the temperature control result in different microstructures. With respect to the loading conditions of steel sheet structures, the influence of the temperature control and process sequence on the fatigue behavior has been analyzed.

In order to characterize the mechanical properties of lap joints, strength is investigated with different testing speeds (quasi-static and crash) and different load angles (tensile and tensile-shear). As testing method, the LWF KSII setup, as described in (DVS 2007), is applied. Additionally, weld performance, failure modes will be validated on structure similar specimen geometry (T-Joint sample). An analysis of the failure modes completes the characterization of the weld seam behavior.

2. Investigation of welding suitability

2.1. Processing conditions

In general for welding of martensitic stainless steels short thermal cycles are preferred. In order to control the hardness loss in the heat affected zone a weld heat treatment adjusted to the material, i.e. mainly it's carbon content is prerequisite. Preheating to martensite start temperature in combination of a suited tempering below the temperature of the dissolution of the alloy carbides will lead to a relaxation of the tetragonal martensite and enhance the ductility of the weld. Pre-heating also leads to an increase of the width of seam and heat-affected zone, that the process becomes less sensitive to maladjustments during manufacturing.

Table 1. Welding parameters

Parameter	CO_2 laser	Disk laser
Beam power P_L/kW	2.5	4
Spot diameter d_F/μm	340	610
Fibre diameter D_F/μm	-	300
Beam diameter D_S/mm	17	-
Focal length f/mm	200	400
Welding speed v_s/ m/min	5	4
Input energy E_s/kJ/min	30	70
Joint type	Square butt joint Lap joint	Lap joint
Sheet thickness d/mm	1.5	
Seam width b_s/mm	0.65	1.1

As beam sources a carbon dioxide laser and a fiber laser were used. Table 1 gives an overview over the parameters attained. In general a preheating to martensite start temperature, an intercooling to 150°C – 200°C after welding tempering with below A_{c1} for martensitic welding is recommended (Schu1z 2000). Martensite start temperature is determined by

$$T_{Ms}\ (°C) = 550 - 360C - 40Mn - 35V - 20Cr - 17Ni - 10Cu - 10Mo - 8W + 15Co + 30Al$$

with the content of the alloying elements given in mass-percent (Bleck 2007).

Tempering of the hardened material requires lower temperature in order to maintain the hardness of the material. For the material 1.4034 (X46Cr13) tempering at 400°C for 5 min was applied. This temperature does not allow carbide dissolution and is sufficient to relax the bct martensite structure. Also the reversion of austenite is limited (Yuan 2012).

Within the frame of the welding tests two manufacturing cases were simulated: (1) the welding of sheets in as-rolled condition followed by press hardening for the production of tailored blanks and (2) welding of the already press hardened sheet metal representing the case of joining in assembly.

Figure 2 shows macro sections of welds at an input energy of 30 kJ/m. In as-rolled condition a slender weld is visible with 80 to 100 μm wide heat-affected zones. Preheating leads to a slight increase of the fused zone width but a big increase of the width of the HAZ to about 200 μm. The welds in hardened material show the same trend.

Additionally different zones are visible in the HAZ. The bright area is characterized by a high hardness whereas the dark zones are tempered to a comparably low hardness. Is the weld press hardened, as in the case of tailored blanks, the heat-affected zone disappeared due to the austenitisation during the hardening process. The fused zone is modified in a way that the dendritic microstructure is transformed to a columnar structure.

2.2. Weld microstructure

The weld microstructure becomes from columnar at low carbon content to dendritic at medium carbon content (0.45 wt.% in 1.4034). Figure 3 shows the microstructure in fusion zone and heat-affected zone for treatment conditions. In figure 3b the micrograph at the fusion line of a weld in as-rolled condition is shown. The area besides the fusion line is characterized by the growth of alloy carbides. With increasing distance from the fusion line the fraction of martensite decreases to the nominal value of the base material.

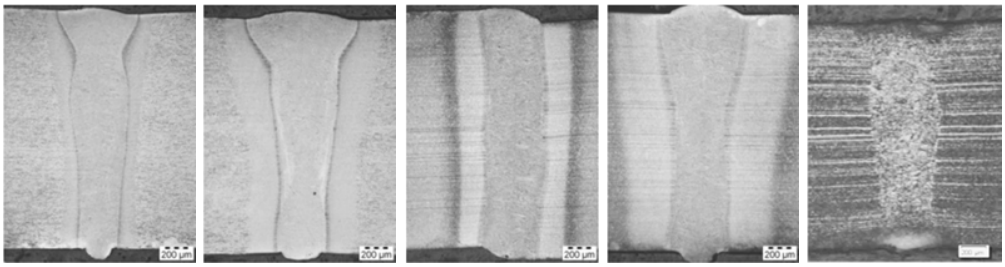

a b c d e

Figure 2: Macro sections of weld seams at input energy of 30 kJ/m under varying pre-heating conditions
a) As-rolled, RT, b) As-rolled $T_{Ms,}$ c) Press hardened, RT, d) Press hardened, $T_{Ms,}$ e) Press hardened after welding

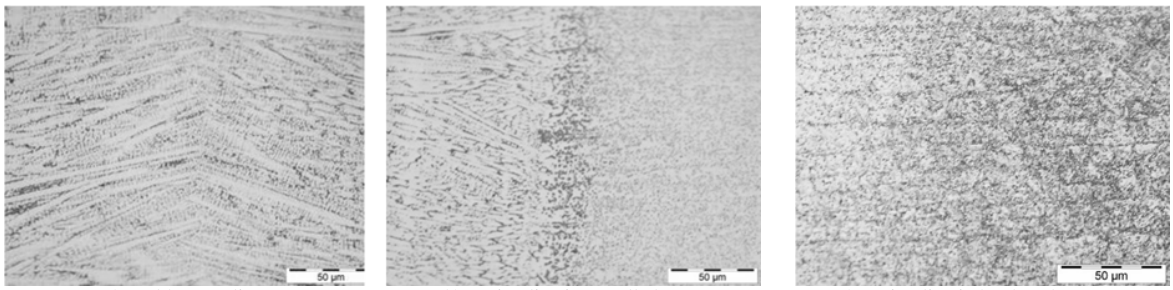

a) Weld centre line b) Fusion line in as-rolled state c) Fusion line in hardened state

Figure 3: Microstructure of the weld zone in 1.4034 in as-rolled condition

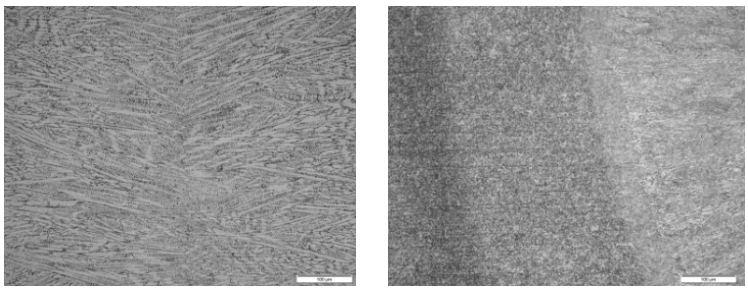

a) Weld centre line b) Fusion line and HAZ (fused zone right)

Figure 4: Micro sections of welds in press hardened material

In figure 4 the microstructure of a weld in hardened material is depicted. At the weld center line (a) a dendritic solidification structure is visible. Due to the initially finer distributed carbides the dendrites appear to be finer with a

smaller spacing. The HAZ consists of four zones. Adjacent to the fusion line a two phase zone consisting of bct martensite and austenite is visible. The second area consists mainly of martensite and is characterized by a local increase of hardness. This martensite changes to a bcc type martensite (tempered) and its fraction decreases with the distance from the fusion line. At the transition to the base material the material is almost fully tempered.

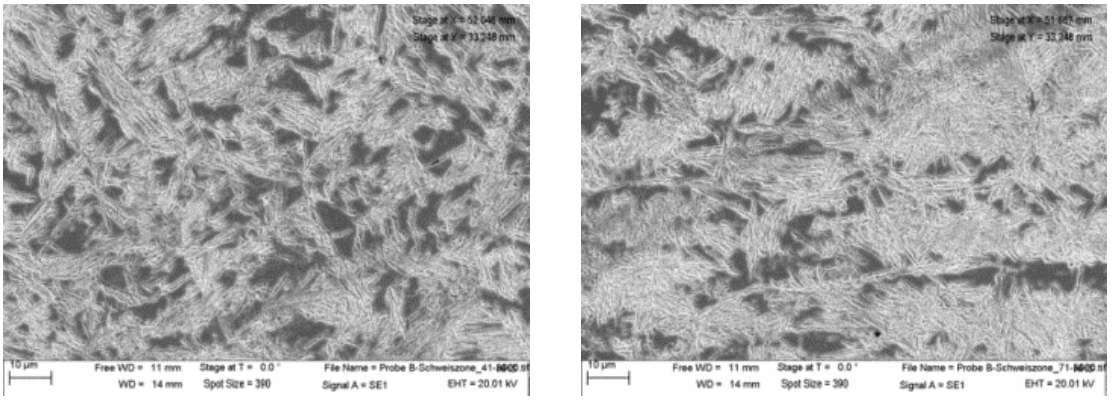

a) Weld centre line b) Former coarse grained zone

Figure 5: Microstructure of the weld zone in 1.4034 hot stamped after welding

Hot stamping changes the microstructure of the fusion zone. Figure 5 shows a martensitic base with about 26% retained austenite (by area fraction). In the heat-affected zone the base metal structure is restored from the fusion line on. It becomes invisible. Slightly increased grain and an increase of 4% retained austenite make the difference against the hardened base metal.

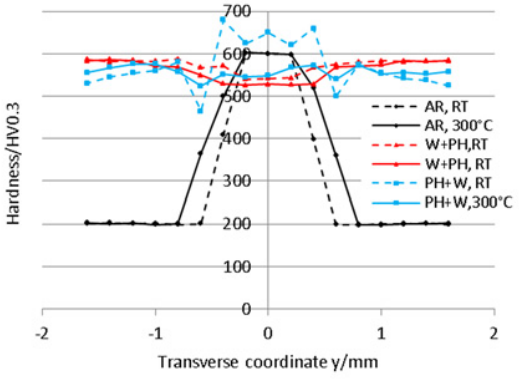

Figure 6: Hardness survey on 1.4034 for different thermal treatments

In figure 6 hardness plots across the weld zone for different thermal treatment of the material are displayed. Measurements were taken using a proof load of 3 N. In the diagram dashed lines correspond to welds produced without pre-heating, solid lines to pre-heating to T_{Ms} = 300°C. Black graphs (rhombs) represent the hardness of welds in as rolled material. A steady increase of hardness in the fusion zone to 600 $HV_{0.3}$ can be observed. The effect of pre-heating is visible in the seam width at the slopes. The blue graphs (squares) represent the hardness of welds in press-hardened material. Without pre-heating a dip in the heat-affected zone by 80 to 110 points is observed. By pre-heating this dip can be much smaller.

After press hardening the welds show different hardness characteristics as shown in the red graphs (triangles). A slight increase in the former heat-affected zone and a decrease in the fusion zone can be measured. Peak hardness was measured to 580 $HV_{0.3}$ at the fusion line. The hardness at the weld centre line is equal to that of the hardened base material 520 $HV_{0.3}$. It should be noted that the values after press hardening are below the values for untempered weld material.

3. Fatigue testing

Therefore cyclic tests with constant amplitudes have been carried out using a resonance pulsator, which enables a test frequency of about 100Hz depending on the specimen's stiffness, and a load ratio $R = 0$ as recommended in (Hobbacher 2008). The failure criterion in the fatigue tests was a crack length of about 0.5mm detected by a test frequency drop off by 1Hz respectively the test was stopped at $N = 1 \cdot 10^7$ cycles. For this fatigue tests the specimen geometry according to (SEP1240) has been modified by a butt joint vertical to the cyclic loading direction. The design of the specimens is depicted in figure 7.

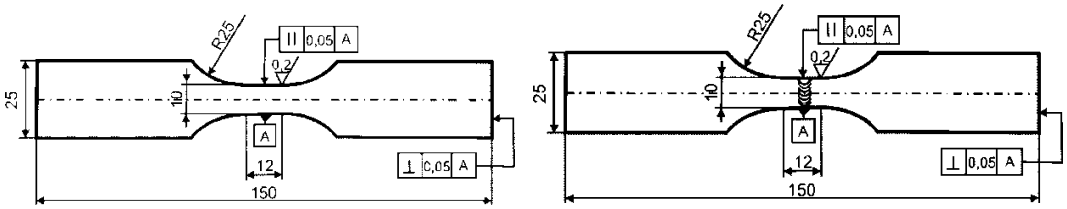

Figure 7: left: Fatigue specimen for the basic material; right: Butt joint fatigue specimen.

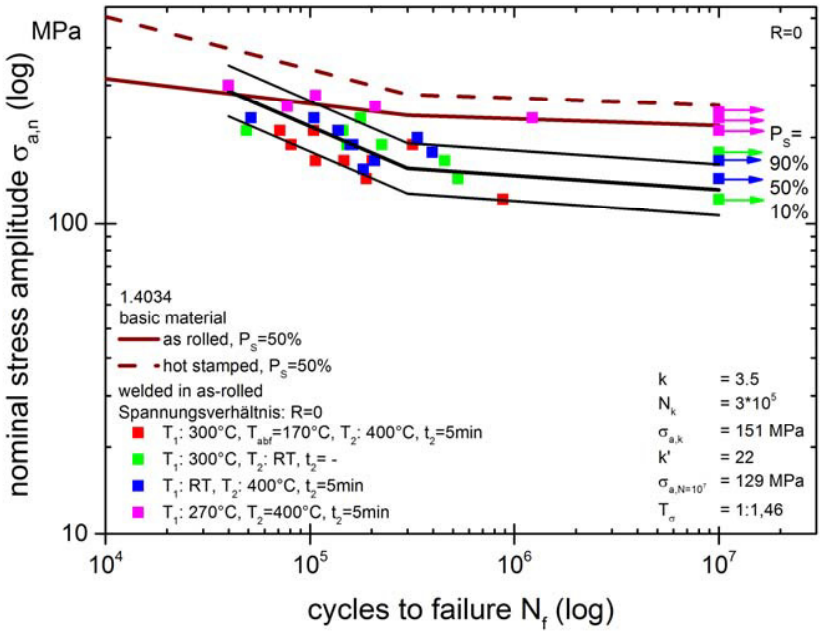

Figure 8: 1.4043 butt joints SN-curves with different heat treatment conditions.

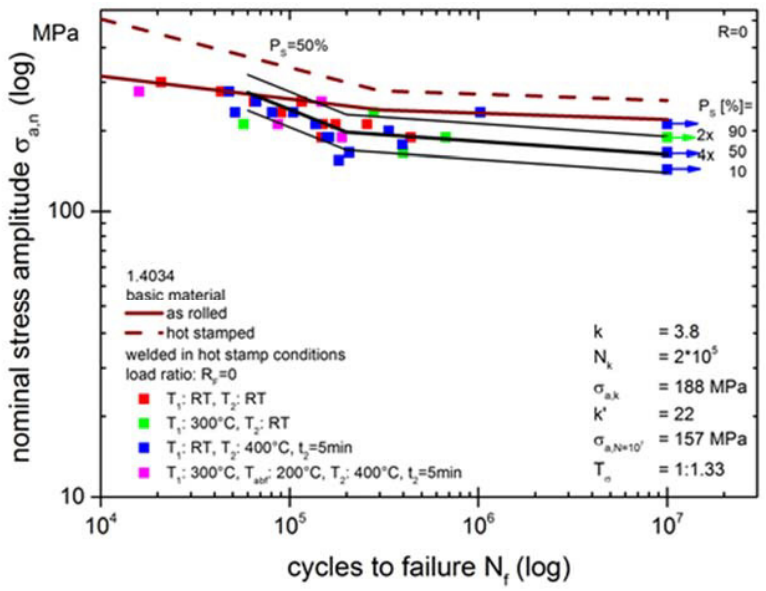

Figure 9: Fatigue strength comparison of different temperature controls for 1.4043 and the application case welding during the assembly.

For the benchmark for the fatigue of butt joints cyclic tests with constant amplitudes with the basic material have been performed. Therefor two different material states were used corresponding to different application cases. The first material state is as-rolled and the second one accords to hot stamped material state which corresponds to the material state in parts and components. The resulting SN-curves reveal the maximum achievable fatigue strength.

3.1. Results

The application case tailored blank represents the welding in as-rolled condition in order to join two steel sheets before the forming and heat treatment. Hence, the reference SN-curve of the application case tailored blank is the as-rolled condition of the basic material. The temperature control during the welding process influenced the resulting fatigue strength. For not optimized welding parameters the SN-curve could be described by a slope of $k = 3.5$ and a knee point at $N_k = 3 \cdot 10^5$ and $\sigma_{a,n,k} = 151$MPa. The Wöhler curves are shown in figure 8.

With well adapted welding parameters regarding the microstructure the fatigue strength of 1.4043 butt joints achieved the fatigue strength of the reference SN-curve that means the fatigue strength of the basic material with the as-rolled state. Compared to the results of the application case tailored blanks an ongoing optimization of temperature control should increase even the resulting fatigue strength for this application case (figure 9).

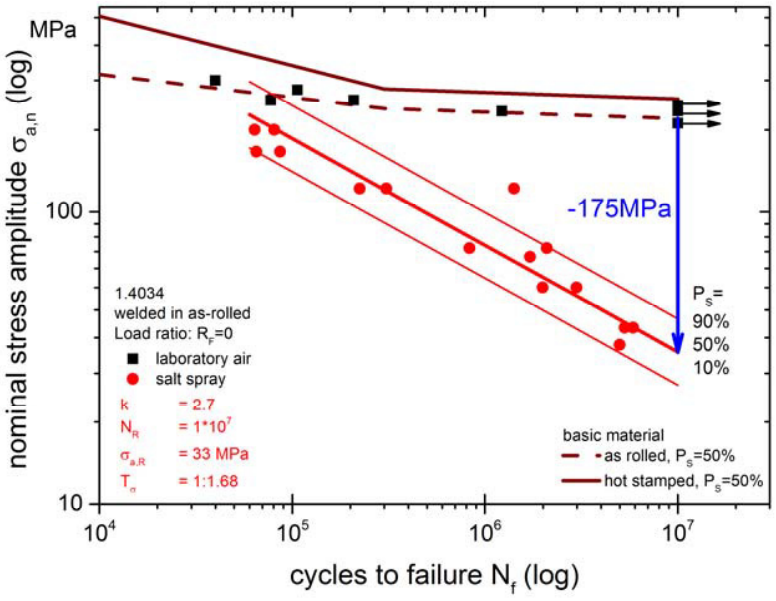

Figure 10: Influence of a salt spray test with 3% NaCl-solution on the fatigue strength of 1.4043 in tailored blanks application case

In order to reveal the effect of environmental condition on the fatigue strength, corrosion fatigue test were carried out. The cyclic loading was superposed by 5 minutes spraying a 3% aqueous solution of sodium chloride with a pH-value in the range of 5.6 to 6.1, followed by 20 minutes without spraying and additional dehydration. For this investigation the specimens of the application case tailored blanks were used. While the fatigue strength at laboratory environmental conditions achieved the fatigue strength of the basic material in the as-rolled state due to the corrosion the fatigue strength decreases. Up to 10^7 cycles no knee point of the SN-curve is detectable, as shown in figure 10. To describe the SN-curve in case of salt spray test a slope of $k = 2.7$ and a reference point at $N_R = 10^7$ cycles and a nominal stress amplitude $\sigma_{a,n} = 33$MPa can be used. Caused by the corrosion the fatigue strength decreased at $N = 10^7$ by about 175 MPa.

4. Testing the structural behavior

The load-bearing behavior as well as the failure modes were tested in KSII tests at lap joints. Deformation rates of 10 mm/min and 2 m/s had been applied for the quasi-static (QS) and the crash case (SA), respectively. Tests were conducted for the case of shear load. The results of the single-element specimens underwent verification tests at a workpiece-like specimens simulating a connection between a B-post, made from press hardened 1.4034, and a rocker panel from 1.0548 (HC340LA). The component was welded with straight welds using a disk laser in order to realize a wide seam.

4.1. Single-element testing

In figure 11 typical displacement-load curves for shear load with the parameter input energy or seam width, respectively, are shown. The load was applied as shear load. The maximum forces vary between 12 and 22 kN at displacements ranging from 0.9 to 2.2 mm. The specimens tested under quasi-static load application show a steeper rise but lower maximum force compared to those tested under abrupt load. This shows a strain-rate dependent material behaviour.

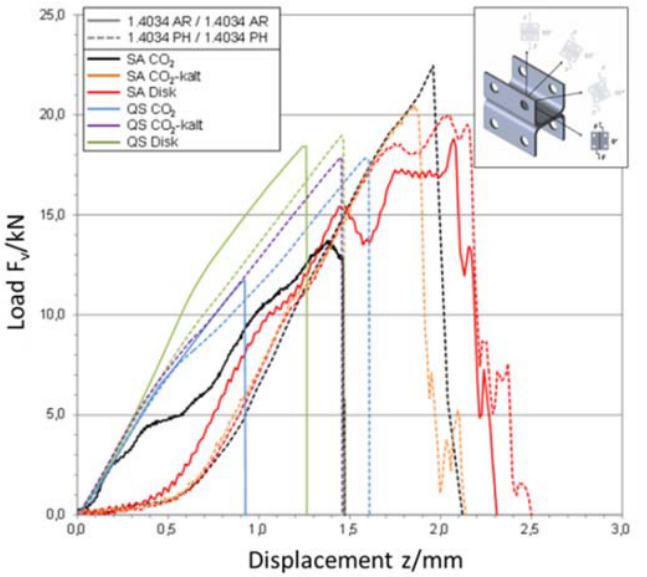

Figure 11: Comparison of the load-displacement curves of as-rolled (solid lines) and press hardened (dashed lines) material under shear load.

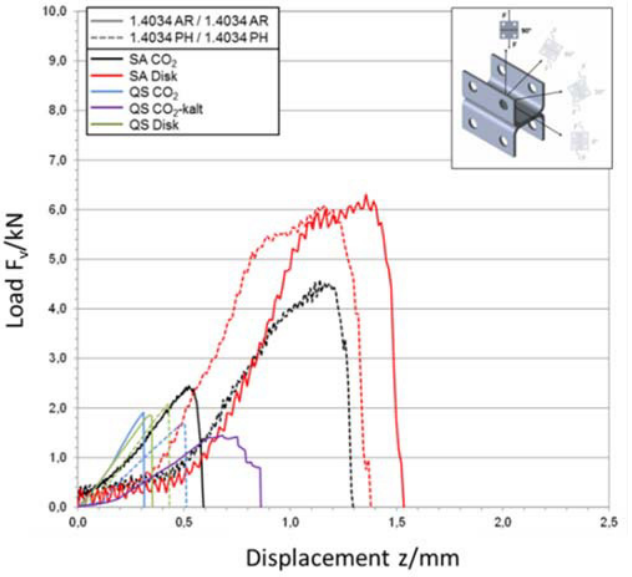

Figure 12: Comparative representation of the displacement-load curves for the case of quasi-static and abrupt normal loading.

At the press hardened specimens similar slopes of the curves for both cases of load applications were determined. A significant difference in the strength of the joint depending on the seam geometry and the input energy cannot be determined. Failure takes place always as a shear fracture in the joint area between the sheets.

The case of normal load is represented in figure 12. Some significant differences become obvious. Highest forces at up to 6 kN are attained in the case of abrupt load application (CR). In this case a strong dependency on the input seam width is determined. The seams welded by the disk laser with a width of about 1.1 mm can bear higher load compared to the narrow CO_2 laser welds (0.8 mm). There is also a significant difference in the latter ones regarding the heat treatment state of the base material. Force and elongation of the press hardened specimens is much smaller compared to those in as-rolled condition.

4.2. Workpiece-like specimen

Figure 13 shows the force-displacement behavior of T-Joint samples for transverse (a) and longitudinal (b) load of 1.4034PH/1.0548 material combination, a failure development sequence for crash load in transverse direction and (c) characteristic failure modes for the considered loads (d). The failure of the T-Joint depends on the load orientation and on the testing speed. Thus, leads to different force values.

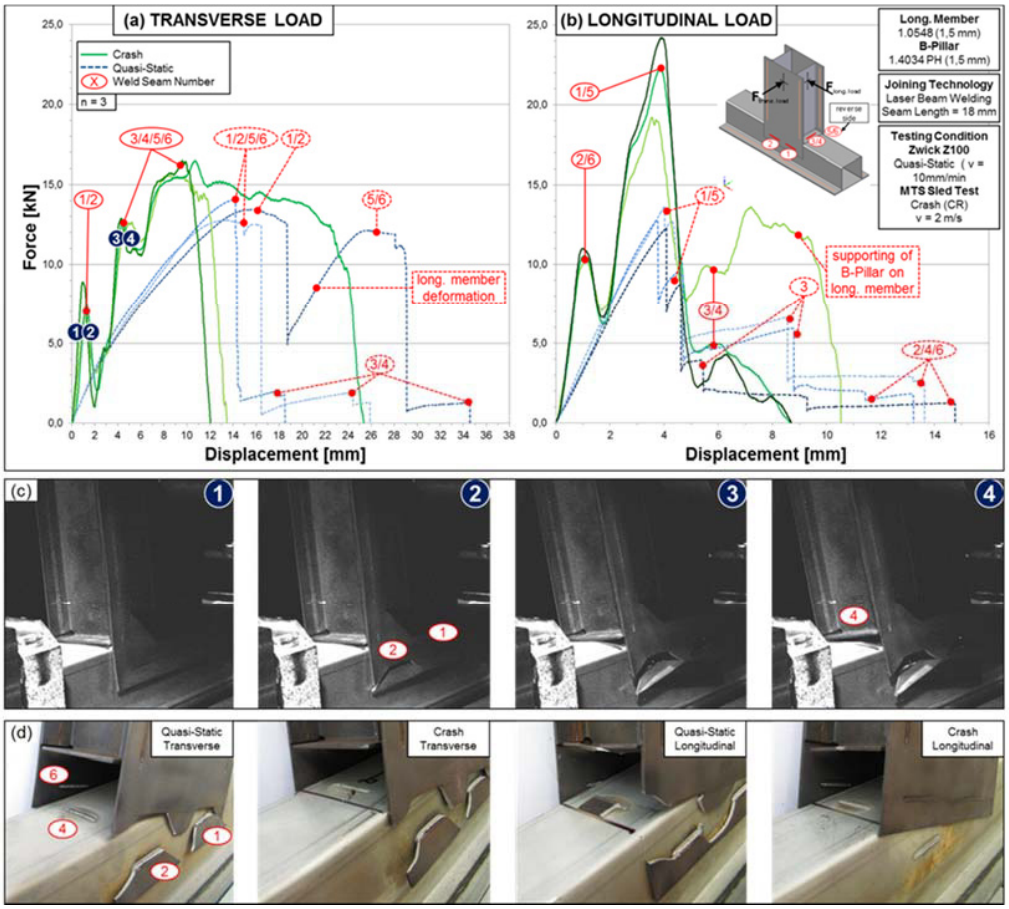

Figure 13: Force-displacement behavior of T-Joint samples (a) for transverse and (b) longitudinal load, (c) selected failure development sequence and (d) failure modes for considered loads.

The force-displacement curve for crash load in transverse direction is characterized by three peaks at different forces. The first peak marks the fracture of the two weld seams in load orientation (weld seam 1 and 2) between the cover plate of the B-Pillar and the longitudinal member (Fig. 13c, 1–2). The crack propagation starts simultaneously for both weld seams at forces of 7–9 kN and the cracks growth throughout the 1.4034PH are accompanied by a sudden drop of the force-displacement curve. The next peak emerges at forces of approx. 12.5 kN. Here, the both weld seams in the two lugs (weld seam 3 and 4) are subjected to a peel load (Fig. 13c, 3–4). The fracture of these weld seams are very brittle and occurs in the zone along the sheet interfaces. The next peak characterizes the maximum force, resulting from a failure of the weld seams opposite to the load orientation (weld seam 5 and 6). This failure is accompanied by a strong deformation of the 1.0548 longitudinal member. This leads to a superposition of bending moments and tensile stresses exerted onto the weld seams.

The force-displacement curves for crash load in longitudinal direction shows two significant peaks. At a displacement of 1 mm and forces of 10–11 kN the first fracture occurs at the weld seams 2 and 6 in consequence of the occurring bending moment and the supporting of the B-post on the longitudinal member, followed by a raise to

the maximum force of 19–24 kN and a fracture of the weld seams 1 and 5. At this particular moment, these weld seams are mainly exposed to tensile shear stresses. Finally, the fracture of the weld seams 3 and 4 occurs at considerable low forces of about 5 kN. One specimen occurs a supporting of the B-post on the longitudinal member, thus, shows an increase of the force in the remainder of the curve. Compared to the crash load in transverse direction, the failure sequence for quasi-static load starts with an almost simultaneous fracture of the weld seams 1/2/5/6 at forces of 12–14 kN. In case of a strong deformation of the longitudinal member, the weld seams 5 and 6 break after large displacement. Final detachment occurs with the fracture of the weld seam 3 and 4 at about 2 kN. Hence, the maximum forces for crash load in transverse direction found to be 20 % greater than for quasi-static load and approx. 50 % higher, for longitudinal orientation, respectively.

The evaluation of the weld performance in a structure similar component indicates different weld seam failure sequences, dependent on the orientation and the speed of the impact. The maximum joint strength capacity of the B-post to the longitudinal member for transverse load attains forces of 13 kN for quasi-static and 16 kN for crash load while for longitudinal load the forces reaches values of 13 kN and 19–24 kN, respectively. It can be shown that suitable and appropriate welding conditions enable the realization of welds with high capacity for load application. Therefore, a general weldability for the considered materials is given. In the quasi-static case maximum loads between 1.5 and 2.3 kN are attained. There is not much change in the load capacity. The results seem to be independent on the case, seam with, material state, and weld heat treatment.

5. Conclusions

Martensitic stainless steels can be welded under a standard weld treatment. In the case of welding tailored blanks a weld heat treatment is not required, but tempering of the weld improves the fatigue properties significantly. In welding of hardened sheets the effect of the heat treatment chosen had a less pronounced effect. With optimum weld heat treatment the fatigue strength of the parent material in as-rolled condition will be attained. In dissimilar welds the values of the crash properties are limited by those of the weaker partner. Crashworthiness depends rather on the seam geometry and the load direction than on the weld heat treatment. With extremely high fracture forces the load-bearing capability of hardened martensitic stainless steels supersedes that of manganese boron steels. The latter show slightly higher fracture forces and better ductility under axial load. In dissimilar welds with conventional deep drawing steels higher strengths were attained than for manganese boron steels. Especially on the tests on component-like specimens it was found that the failure mode does not only depend on the load rate but also on its direction. Regarding the performance an exact knowledge of the loading mode is required for an optimum application of the materials.

Acknowledgements

In this paper, selected results of the funded research projects P905 (IGF 17.433 N) were presented. The IGF project 17.433 N (P905) of the research association Forschungsvereinigung Stahlanwendung e.V.—FOSTA, Sohnstrasse 65, 40237 Düsseldorf was funded by the AiF under the program for the promotion of joint industrial research and development (IGF) by the German Federal Ministry of Economic Affairs and Energy based on a decision of the German Bundestag.

References

Bleck, W. (2007). Material science of steel. Department of Ferrous Metallurgy, RWTH Aachen University

Costa, L.; Colaçao, R.; Réti, T.; Deus, A.M.; Vilar, R., 2013. Tempering effects in steel parts produced by additive fabrication using laser powderdeposition; Proceedings of the 1st International Conference on Advanced Research in Virtual and Rapid Prototyping, 1st-4th October 2003, Leiria, Portugal

Dahmen, M., Han, X., Sun, Z. (2012). Laser beam welding of Martensitic stainless steels as-rolled and under press-hardening conditions. IIW Regional Congress, Johannesburg, November 7 – 8, 2012 Congress Proceedings

Dahmen, M., Janzen, V. Lindner, S., Wagener, R. (2014). Laser beam welding of ultra-high strength chromium steel with martensitic microstructure. 8th International Conference on Photonic Technologies LANE 2014, Physics Procedia 56 (2014) 525 – 534

DVS/EFB 3480-1, 2007. Prüfung von Verbindungseigenschaften—Prüfung der mechanisch kombiniert mittels Kleben gefertigter Verbindungen. Instruction sheet of DVS/EFBCommittee „Mechanisches FügenB, DVS Media, Düsseldorf

Hobbacher, A. (2008). Recommendations for Fatigue Design of Welded Joints and Components. International Institute of Welding (IIW), IIW document IIW-1823-07 ex XIII-2151r4-07/XV-1254r4-07. Paris

Schulze, G., 2010. Die Metallurgie des Schweißens. Springer Verlag, Berlin Heidelberg, p. 422-424

SEP1240, 2006. Stahl-Eisen-Prüfblatt (SEP) des Stahlinstitut VDEh, SEP1240, 1st Edition: Testing and Documentation Guideline for the Experimental Determination of Mechanical Properties of Steel Sheets for CAE-Calculations. Stahleisen Verlag, Düsseldorf

Yuan, L.; Ponge, D.; Wittig, J.; Choi, P.; Jiménez, J. A.; Raabe, D. (2012). Nanoscale austenite reversion through partitioning, segregation, and kinetic freezing: Example of a ductile 2 GPa Fe-Cr-C steel. Journal: Acta Materialia, Elsevier Ltd., Vol. 60, Issues 6-7, 2012, p. 2790-2804